PNAS
www.pnas.org

Supplementary Information for

The neuropeptide allatostatin C from clock-associated DN1p neurons generates the circadian rhythm for oogenesis

Chen Zhang, Ivana Daubnerova, Yong-Hoon Jang, Shu Kondo, Dušan Žitňan and Young-Joon Kim

Correspondence and requests for materials should be addressed to Young-Joon Kim (kimyj@gist.ac.kr).

This PDF file includes:

Supplementary Materials and Methods
Figures S1 to S9
Tables S1, S2
SI References

Supplementary Materials and Methods

Fly stocks. Fly lines were raised at 25°C and 60% humidity under a 12 h:12 h light:dark cycle on standard fly media. The following stocks were reported previously: *AstC-R1-Gal4* (1), *AstC-R2-Gal4* (1), *Ccap-GAL4* (2), *CRZ-GAL4* (3), *dilp2-GAL4* (4), *EH-GAL4* (5), *Hugin-GAL4* (6), *NPF-Gal4* (7) *PDF-GAL4*(8), *SIFa-GAL4* (9), *Pburs-GAL4* (10), *otdFLP* (11), *UAS > stop >mCD8GF* (12), *UAS>stop>dTrpA1* (13), *UAS-dTrpA1* (14), *nSyb-Gal4* carrying *UAS-Dicer2* and *UAS-mCD8-GFP* (gift from Barry J. Dickson, Janelia Research Campus), *JHAMT-Gal4* (15), y^2cho^2 v^1*;attP40{nos-Cas9}/CyO* (16) (CAS-0001). The following stocks were obtained from the Bloomington *Drosophila* Stock Center (BDSC), the Vienna *Drosophila* RNAi Center (VDRC), or the Korean Drosophila Resource Center (KDRC): *89y-GAL4* (BDSC #30817), *36y-GAL4* (BDSC #30819), *UAS-Dicer2* (BDSC #24648), *NPF-GAL4* (BDSC #25682), *AstC-IR1* (VDRC #13772), *AstC-IR2* (VDRC #102735), *Dh31-IR1* (VDRC #50293), *Dh31-IR2* (VDRC #37763), *Dh31-IR3* (VDRC #37764), *per-IR1* (BDSC #40878), *per-IR2* (BDSC #31285), *AstC-R1-IR1* (VDRC #13560), *AstC-R1-IR2* (BDSC #JF02656), *AstC-R2-IR1* (BDSC #JF01960), *AstC-R2-IR2* (VDRC #50000), *Amn-GAL4* (KDRC #10010), *AstA-GAL4* (KDRC #10016), *AstC-GAL4* (KDRC #10012), *Burs II3-GAL4* (KDRC #10049), *CCHa1-GAL4* (KDRC #10021), *Dms-GAL4* (KDRC #10006), *Dsk-GAL4* (KDRC #10014), *dilp4-GAL4* (KDRC #10011), *dilp6-GAL4* (KDRC #10013), *dilp7-GAL4* (KDRC #10019), *ETH-GAL4* (KDRC #10018), *ITP-GAL4* (KDRC #10015), *Kinin (drosokinin)-GAL4* (KDRC #10003), *Mip-GAL4* (KDRC #10002), *Nplp1-GAL4* (KDRC #10008), *Nplp2-GAL4* (KDRC #10023), *Nplp4-GAL4* (KDRC #10022), *Orchokinins-GAL4* (KDRC #10005), *Ptth-GAL4* (KDRC #10009), *proctolin-GAL4* (KDRC #10004).

Molecular biology. We generated *CNMa-Gal4* via recombineering. We inserted the Gal4 ORF into the CNMa ATG start site in a recombineering-ready, pre-mapped genomic BAC clone (Clone ID, CH321-34F01) from the P[acman] library (17). Briefly, we first generated the pME[Gal4.2::VP16] plasmid by cloning a *Drosophila* codon-optimized Gal4.2::VP16 sequence from the pBPGAL4.2::VP16Uw vector into pDONR221, which contains an FRT-flanked neomycin resistance cassette (FRT-NeoR-FRT). pME[Gal4.2::VP16] was further modified by adding KpnI and BglII restriction sites for insertion of homology arms, which target the BAC clone of interest. To prepare a CNMa-specific targeting vector, ~500 bp left (LA) and right (RA) homology arms derived from nucleotides flanking the ATG start codon of the CNMa gene were PCR amplified from the BAC clone CH321-34F01 with a pair of KpnI-CNMaLA forward and reverse primers, and a pair of BglII-CNMaRA forward and reverse primers, respectively. Each homology arm was then inserted into the KpnI (for LA) or BglII (for RA) sites of pME[Gal4.2::VP16]. pME[Gal4.2::VP16] carrying the homology arms was PCR-amplified with a pair CNMa LA forward and CNMa RA reverse primers to generate the 3,850 bp-long targeting PCR product carrying Gal4.2::VP16 CDS and a FRT-NeoR-FRT cassette flanked by CNMa-specific homology arms. The targeting PCR

product was then used to transfect *E. coli* EL250 cells carrying the ~90-kb BAC clone CH321-34F01. Homologous recombination between the targeting PCR product and the BAC clone introduced the Gal4.2::VP16 sequence into the ATG codon of the CNMa gene in the BAC clone. The NeoR cassette was then removed by inducing Flp recombinase in EL250 cells to generate the final CNMa-GAL4 construct. This *CNMa-Gal4* construct was then inserted into a specific site on the third chromosome (VIE-49b, a gift from Barry J. Dickson, Janelia Research Campus) using the ΦC31 system (18).

U*AS-AstC* was generated by cloning the NotI-AstC-ORF-KpnI fragment amplified from the cDNA clone RH36507 (AY070699) into the SST13 vector, and then inserting it into a specific site on the third chromosome (VIE-49b. a gift from Barry J. Dickson, Janelia Research Campus) using the ΦC31 system.

The *AstC* and *CNMa* mutant alleles were generated via the CRISPR/CAS9 system. To generate a precisely-defined microdeletion allele for each gene, two CRISPR target sites flanking the coding exons for each gene were selected using TargetFinder (19) and E-CRISP (20). Each CRISPR construct was generated by annealing sense and anti-sense oligos (Table S2) and cloning the resulting double-stranded DNA into the BbsI site of pU6-BbsI-chiRNA. We injected two CRISPR constructs for each gene (250 ng/μL each) simultaneously into y2 cho2 v1; attP40{nos-Cas9}/CyO fly embryos, which express Cas9 in their germ cells. All primers or oligonucleotides used in this study are listed in Table S2.

Bioassays. All assays were repeated on at least two different days. For the egg-laying assay, we modified a published protocol (21). Flies were raised on normal fly food at 25°C in a fly room under a 12h:12h, light: dark cycle. Flies were collected immediately after eclosion. Females were aged in groups for 3 days, and *CS* males were aged individually for 4 days. Single naïve *CS* male and virgin test female flies were placed in 1 cm diameter chambers for copulation. Females that copulated were transferred individually into vials containing normal fly food for 48 hours. Then, the number of eggs laid by each female was counted. For thermal activation, mated females were transferred to a 21°C or 30°C incubator immediately after copulation.

For the egg-production assay, freshly eclosed females were placed individually in vials for three days at either 21°C or 30°C. Then, their ovaries were dissected in phosphate buffered saline (PBS) and the mature eggs (stage 14) in both ovaries were counted under a stereomicroscope. Images of the ovaries were taken using a LEICA EZ4E and the LAS V4.10 program. To examine the circadian vitellogenesis rhythm, we modified methods described by Allemand (22). Groups of 5 test females and 6 *CS* males cultured under LD 12:12 were collected immediately after eclosion and kept in food vials for 1 day under LD 12:12, 25°C. They were then transferred and kept in

constant darkness for 5 days with a transfer to fresh food vials on day 5. On day 6, the ovaries were dissected in PBS every two hours. The ovarioles were separated and the stages of the vitellogenic follicles were determined according to Jia et al., 2016 (23).

For the oviposition assay, post-mating females were placed either at 21°C or 30°C for 48 hours. Then, their reproductive organs were dissected and the mature eggs (stage 14) from both ovaries were counted under a stereomicroscope. Images of the ovaries were taken using a LEICA EZ4E and the LAS V4.10 program.

For the ovulation assay, post-mating females were placed either at 25°C or 30°C for 24 hours. Then, their reproductive organs were dissected and each uterus was scored for the rate at which it contained a mature egg (mature egg=100, no mature egg=0).

Methoprene treatment. Methoprene (Sigma-Aldrich, catalog number 40596-69-8) was dissolved in 95% ethanol (1 µg/µl) and added to warm fly food medium (in liquid state) to a final concentration of 1.04 µl/ml (24). Flies were fed food with 1.04 µl/ml methoprene or 1 µl/ml 95% ethanol (vehicle control) individually for 3 days after eclosion.

Immunohistochemistry. After dissecting each CNS in PBS, they were fixed in 4% paraformaldehyde for 20–30 min at room temperature. After washing them in PBST, the samples were incubated with rabbit anti-GFP antibody (1:1000; Invitrogen, A11122), rabbit anti-AstC antibody (25), anti-Dh31 (2) (a gift from Jan Veenstra from Université de Bordeaux), anti-PER (26) (a gift from Eun Young Kim from Ajou University School of Medicine), anti-Dilp2 (27) (a gift from Yu Kweon from Korea Research Institute of Bioscience and Biotechnology), and mouse anti-nc82 antibody (1:50; Developmental Studies Hybridoma Bank) for 48 hours at 4°C. Alexa Flour 488-labeled goat anti-rabbit IgG (1:1000; Invitrogen, A11008) and Alexa Fluor 568 goat anti-mouse IgG (1:1000; Invitrogen, A11004) were used as secondary antibodies for 24 hours at 4°C. Confocal images were acquired with a Zeiss LSM700/Axiovert 200M (Zeiss) or TCS SPE (Leica) and processed with a maximum intensity Z-projection algorithm using Image J (28). To quantify anti-Dilp2 fluorescence, maximum intensity Z-projections of 15 consecutive confocal stacks (5 µm-thick each) covering all somas of 14 IPCs were merged with Image J. Then, the relative anti-Dilp2 fluorescence intensity of each brain was calculated by setting the average of control brains (*UAS-dTrpA1/+*) (for Fig 3J) *or CNMa-Gal4/UAS-dTrpA1, AstC^{1}/AstC^{1}* brains (for Fig 3K) as 100%.

***In situ* hybridization.** After dissecting each CNS and fixing them in 4% paraformaldehyde overnight at 4°C, they were stored in 70% ethanol until being washed with PBS and Tween-20,

treated with proteinase K and glycine, and hybridized with a digoxygenin (DIG)-labeled single-stranded DNA probe overnight at 48°C. After blocking the tissues with 1% BSA, they were incubated overnight at 4°C with an anti-DIG antibody conjugated with alkaline phosphatase (Roche) before being stained with NBT-BCIP (Roche). The primers used to produce the *in situ* probes for AstC appear in Table S2. Images were acquired with a bright field microscope (Olympus BX53). For the projection images of the brain and VNC, several images from different optical Z-sections were acquired, manually inverted, processed with a maximal intensity Z-projection algorithm and then re-inverted using Image J (28).

RT-qPCR. Total RNA was extracted from whole adult female bodies (n = 15) using Trizol (Takara) according to the manufacturer's instructions. RNA (1 µg) was reverse transcribed with oligo(dT) primers (Promega) and Accupower RT premix (Bioneer). Quantitative RT-PCR reactions were performed in 10 µl reaction volumes using an IQTM5 real-time PCR detection system (Bio-rad) with SYBR Premix ExTaq (Takara) according to the manufacturer's instructions. The gene-specific primers for Rp49 and Kr-h1 described previously (29) were used for controls (Table S2).

Wing size measurement. Right wings of 3-day old female flies were dissected and mounted in 70% glycerol. Images of each wing were taken using a LEICA EZ4E and the LAS V4.10 program. The distance between wing landmarks #5 and #13 was measured as previously described (30) with ImageJ and used as an indicator of wing size.

Statistical analysis. GraphPad Prism 5 (GraphPad) was used for all data analysis, except the cosinor analysis. For the cosinor analysis, we used MetaCycle (31).

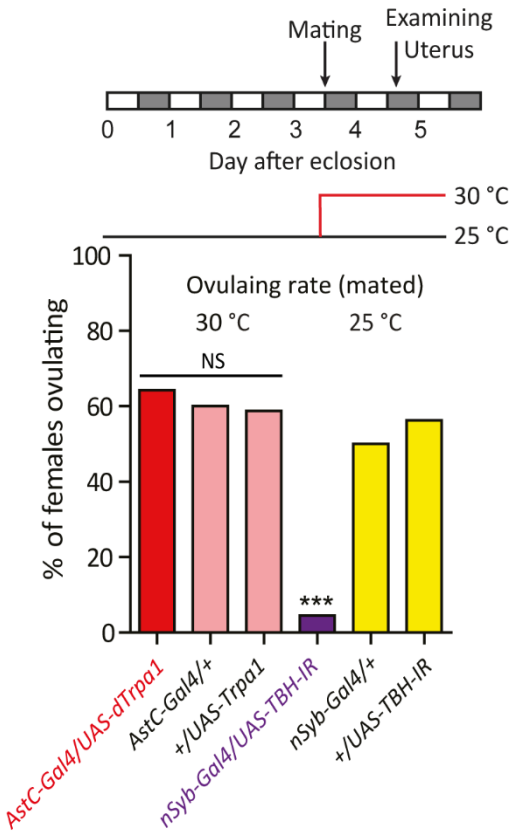

Fig. S1. *AstC-Gal4* neurons regulate oviposition, but not ovulation.

Above, protocol for the ovulation assay. Below, % ovulation frequency of females (*n*=20–40) of the indicated genotypes mated at 25ºC and kept at 30°C and 25°C. One-way ANOVA followed by Tukey's test for multiple comparisons; NS (non-significant, p>0.05) and ****p* < 0.001 for comparisons of *AstC-Gal4/UAS-dTrpA1* (red bar) and *nSyb-Gal4/UAS-TBH-RNAi* (purple bar), respectively, with their parental controls (light red bars or yellow bars, respectively).

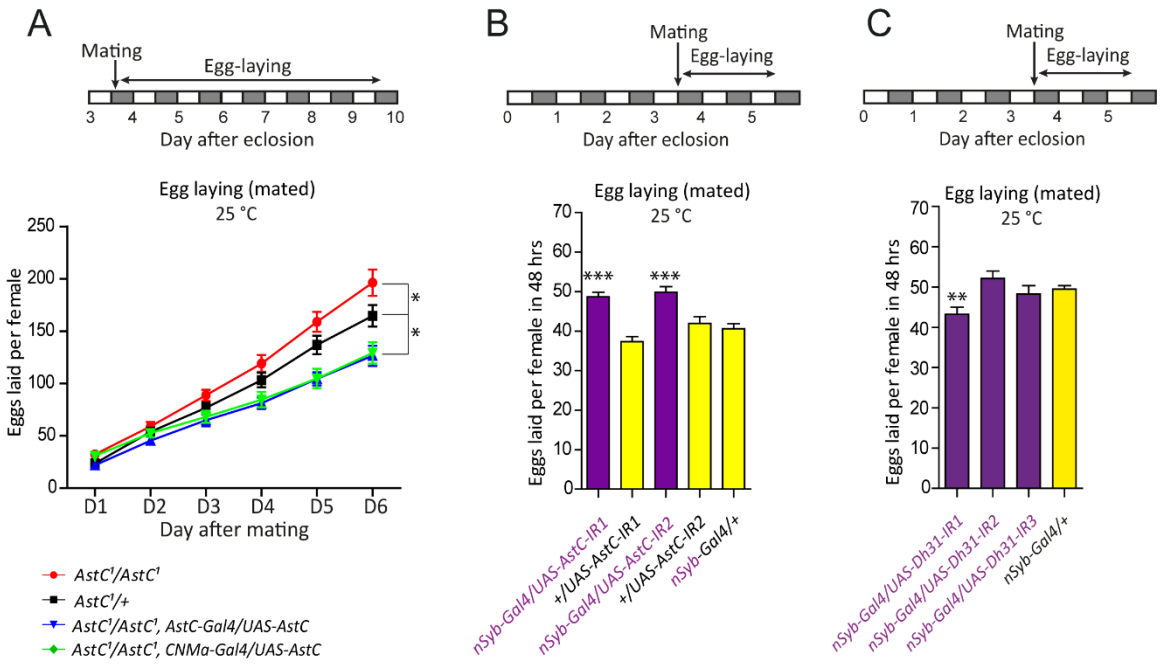

Fig. S2. The role of AstC and Dh31 in female fecundity.

(A) Above, behavioral protocol for measuring cumulative egg laying for 6 days post-copulation. Below, cumulative number of eggs laid per female (n=20–40) of the indicated genotype 1–6 days after mating at 25°C. The means ± SEM of the data are shown. One-way ANOVA followed by Tukey's test for multiple comparisons; *$p < 0.05$.

(B) Above, behavioral protocol for measuring mated female egg laying. Below, number of eggs laid per female (n=20–40) of the indicated genotype kept for 48 hours after mating at 25°C. The means ± SEM of the data are shown. One-way ANOVA followed by Tukey's test for multiple comparisons; ***$p < 0.001$

(C) Above, behavioral protocol for measuring mated female egg laying. Below, number of eggs laid per female (n=40–60) of the indicated genotype kept for 48 hours after mating at 25°C. The means ± SEM of the data are shown. Dunnett's test; **$p < 0.005$ for comparisons against *nSyb-Gal4* alone (yellow bar)

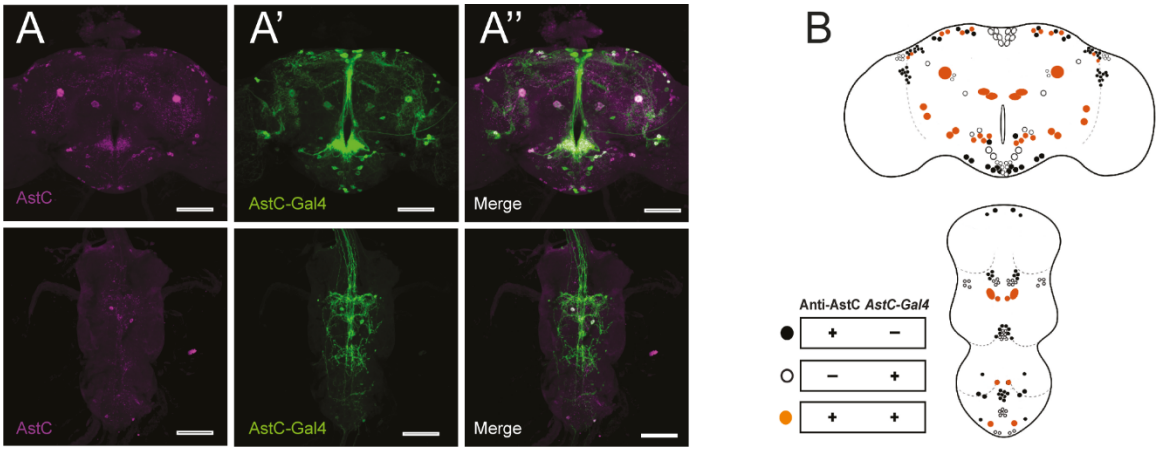

Fig. S3. *AstC-Gal4* drives expression in around 40 neurons in the CNS that express AstC peptide.

(A) A maximum intensity Z projection image of confocal stacks of the brain (upper) and the VNC (bottom) from *AstC-Gal4/UAS-mCD8-EGFP* females stained with anti-GFP (green) and anti-AstC (magenta) antibodies. Scale bar, 50 μm

(B) A cartoon that summarizes the results shown in A''. Circles indicate the CNS cells positive exclusively for anti-AstC (filled circles) or *AstC-Gal4* (open circles). There are 32 and 8 neurons positive for both *AstC-Gal4* and anti-AstC (orange circles) in the brain and the VNC, respectively.

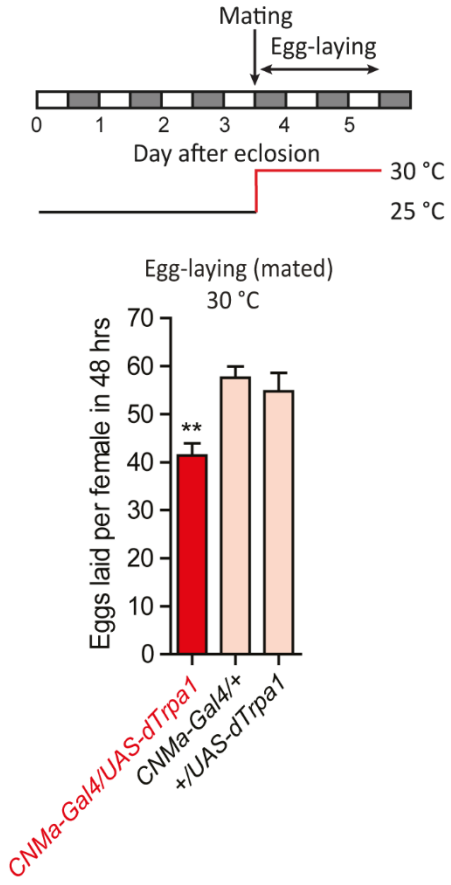

Fig. S4. Activation of *CNMa-Gal4* neurons reduces female fecundity.

Above, behavioral protocol for measuring mated female egg laying. Below, number of eggs laid per female (n=40–60) of the indicated genotype over 48 hours at 30°C. The means ± SEM of the data are shown. One-way ANOVA followed by Tukey's test for multiple comparisons; $^{**}p < 0.005$ for comparisons of *CNMa-Gal4/UAS-dTrpA1* (red bar) to their parental controls (light red bars).

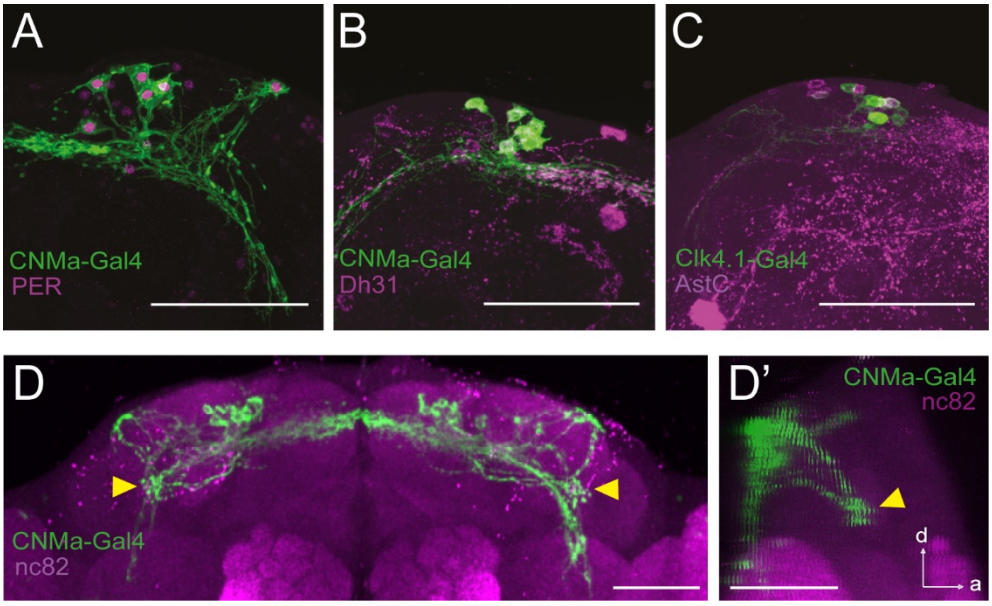

Fig. S5. AstC from AstC-DN1p regulates female fecundity.

(A-C) Dorso-lateral area of the brain indicated by the red box in (Fig 3B) from (A) a *CNMa-Gal4/UAS-mCD8-EGFP* female CNS stained with anti-PERIOD (magenta) and anti-GFP (green) antibodies, (B) a *CNMa-Gal4/UAS-mCD8-EGFP* female CNS stained with anti-Dh31 (magenta) and anti-GFP (green) antibodies, and (C) a *Clk4.1-Gal4/UAS-mCD8-EGFP* female CNS stained with anti-AstC (magenta) and anti-GFP (green) antibodies Scale bar, 50 μm.

(D) A Z-projected confocal image that shows the dorsal area of the brain from a *CNMa-Gal4/UAS-mCD8-EGFP* female CNS stained with anti-GFP (green) and anti-nc83 (magenta; a neuropile marker) antibodies. The brain is oriented with the dorsal surface facing up. (D') A Y-projected image of the z-stack confocal images used to generate (D). This sagittal plane image shows the anterior projection of AstC-DN1p. Yellow arrowheads indicate the AOTU region innervated by EGFP-positive AstC-DN1p processes. White arrows labeled with d and a indicate dorsal and anterior orientations. respectively. Scale bar, 50 μm.

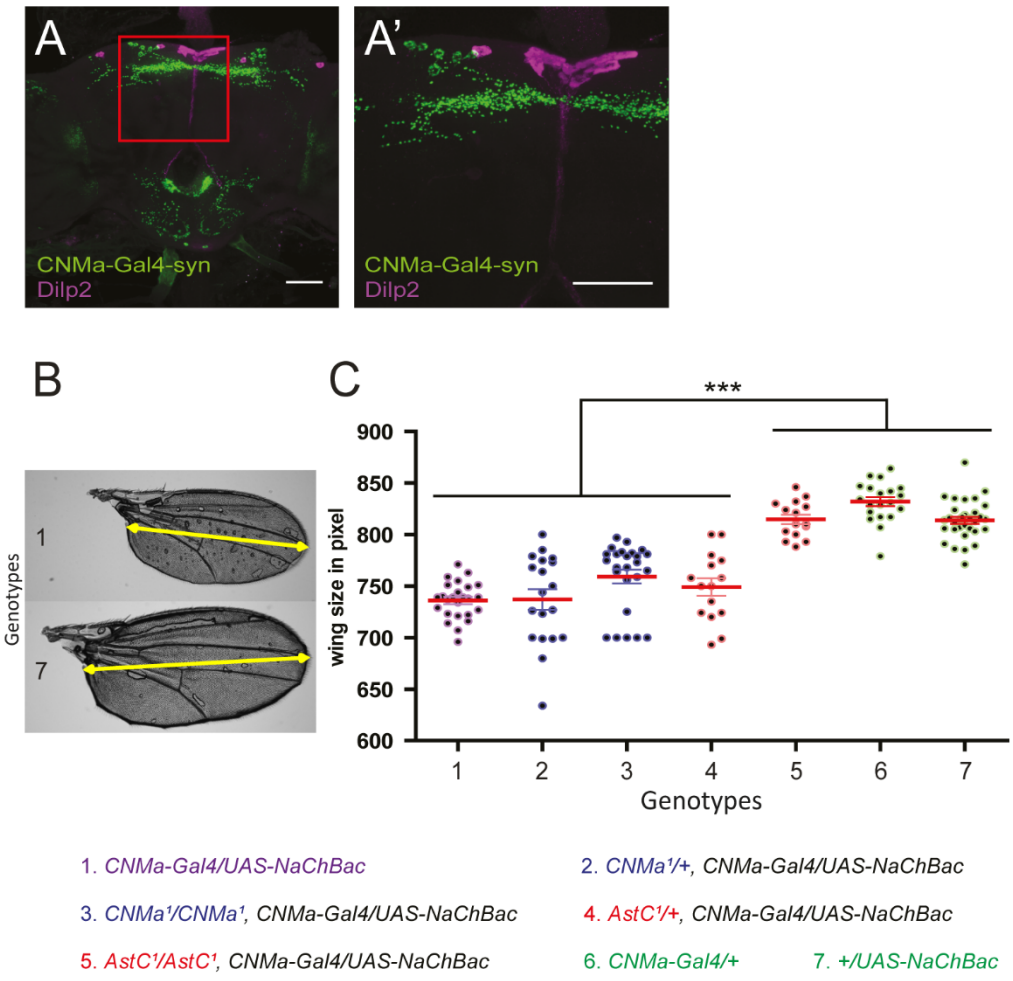

Fig. S6. AstC from AstC-DN1p regulates IIS and developmental growth.

(A) CNS of 4-day-old virgin females from *CNMa-Gal4/UAS-syt-EGFP* stained with the anti-Dilp2 (magenta) and anti-GFP (green) antibodies. Scale bar, 50 μm. (A') The area of the brain indicated by the red box in (E) from a *CNMa-Gal4/UAS-syt-EGFP* female CNS stained with anti-Dilp2 (magenta) and anti-GFP (green) antibodies. Scale bar, 50 μm.

(B) Right wings of 5-day old females from the indicated genotypes. Yellow lines indicate distance between wing landmarks #5 and #13 (30), which are used for wing size identification.

(C) Wing size in pixels as measured in the indicated genotypes. One-way ANOVA followed by Tukey's test for multiple comparisons; ***$p < 0.001$ for comparisons of genotypes 1–4 against other groups. 1 pixel is close to 2.5 μm.

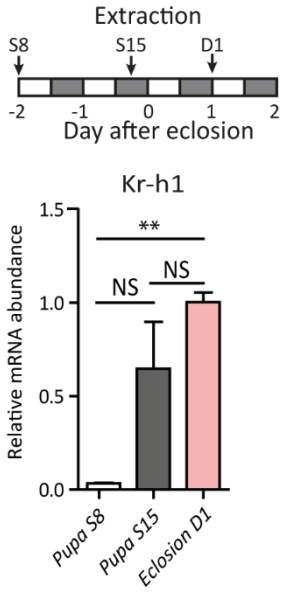

Fig. S7. Level of Kr-h1 in pupal and adult female *Drosophila*

Above, protocol for fly preparation for RT-PCR. Below, Kr-h1 transcript levels in wild type stage-8 pupae, stage-15 pupae, and 1-day-old adult females. The means ± SEM of the data are shown. One-way ANOVA followed by Tukey's test for multiple comparisons; $^{**}p < 0.005$, NS (non-significant, $p>0.05$).

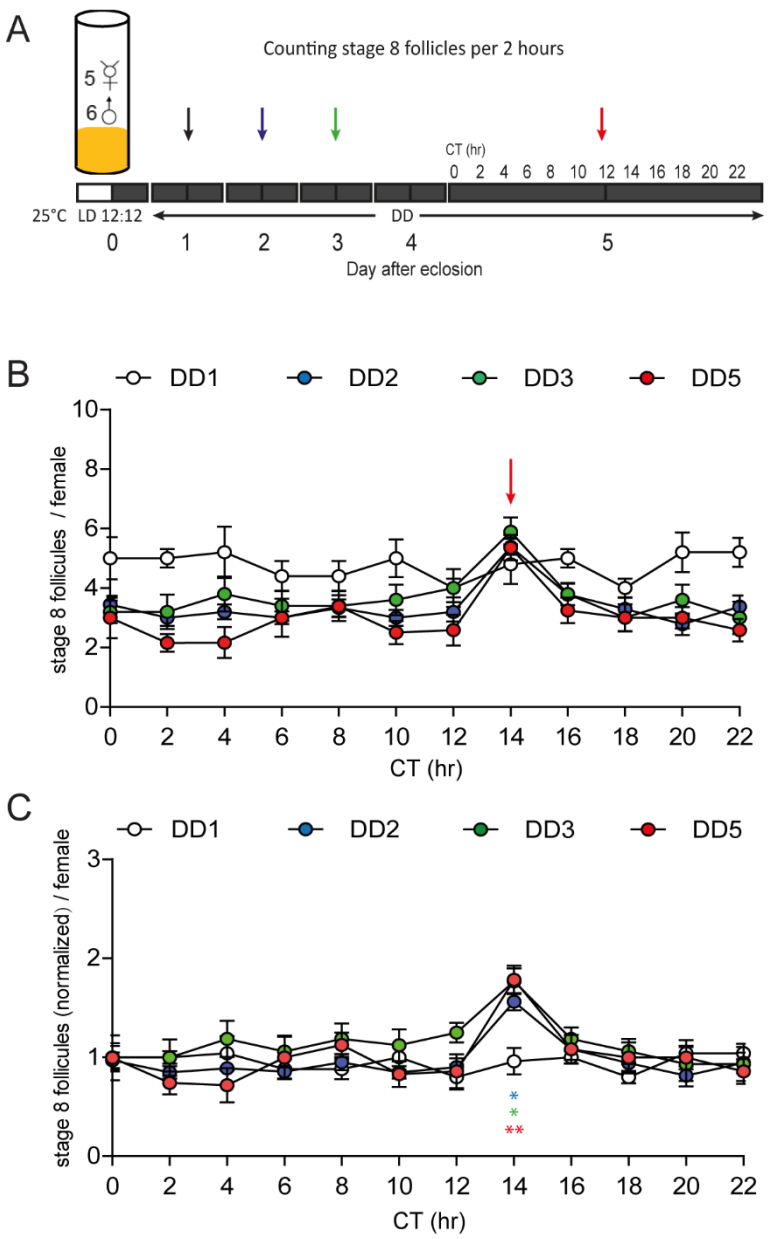

Fig. S8. Circadian vitellogenesis rhythm observed in the control w^{1118} strain

(A) Protocol for measuring circadian vitellogenesis rhythm in B. Groups of 5 virgin females of the indicated genotypes and 6 CS males cultured under a 12:12 LD cycle were placed in food vials upon eclosion and then transferred to constant darkness (DD) on day 2. Over 5 days (except on DD4), the ovaries were dissected every two hours and stage 8 follicles were counted.

(B) The number of stage 8 follicles from the indicated genotypes at the indicated circadian time. In each circle, n = 6-10. An arrow (red) highlights a sudden and temporary elevation in the number of stage 8 follicles at CT14 in DD2, 3, and 5, but not in DD1.

(C) The data from (B) was normalized by the number of follicles at CT0. The means + SEM of the data are shown. One-way ANOVA followed by Tukey's test for multiple comparisons between DD1 and DD2, 3, or 5 at each time point; ***$p < 0.001$; **$p < 0.005$; *$p < 0.05$; no labeling, $p > 0.05$. The symbol for p value is color-coded according to DD2, 3, or 5 used for comparison against DD1.

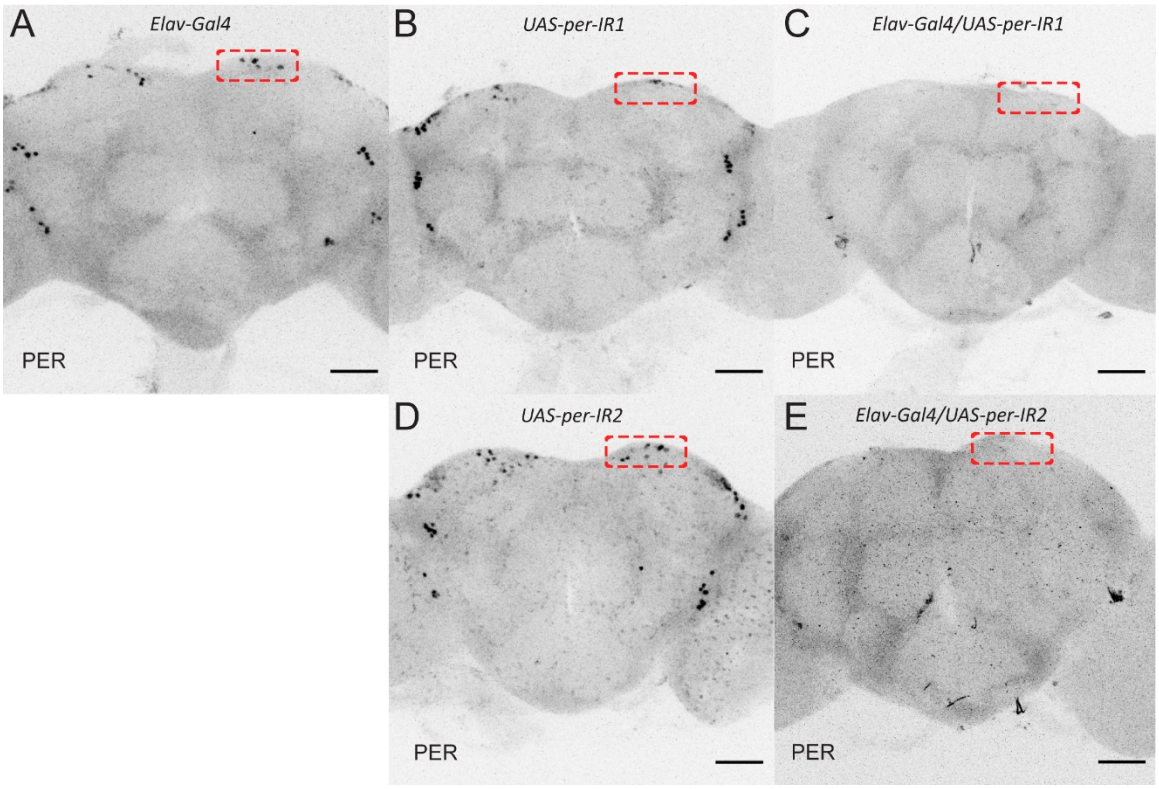

Fig. S9. Pan-neuronal *per-RNAi* almost completely abolished anti-PER immunoreactivity in the brain. (A-E) Color-inverted Z-projected fluorescent confocal images showing brains of the indicated genotypes dissected at ZT23 and stained with anti-PER antibody. Anti-PER labeled somas appear in black. Dotted boxes (red) indicate the dorsal brain area where DN1s reside. Scale bar, 50 μm.

Table S1. Cosinor analysis of vitellogenesis rhythm of the indicated genotype under DD condition. Related to Fig. 4 and Fig. S8.

Genotype*	meta2d_period	meta2d_pvalue	meta2d_AMP	meta2d_rAMP
w^{1118} (DD1)	24	1	0.093399625	0.088881483
w^{1118} (DD2)	24	0.012625144	0.220900319	0.220900319
w^{1118} (DD3)	24	0.00781646	0.31034564	0.267759695
w^{1118} (DD5)	24	0.021677449	0.263936979	0.263936979
Elav-Gal4/UAS-per-IR1	24	0.954047889	0.102482189	0.102482189
+/UAS-per-IR1	24	0.463655095	0.166542007	0.165576146
Elav-Gal4/UAS-per-IR2	24	1	0.019527475	0.019527475
+/UAS-per-IR2	24	0.008119759	0.284578883	0.228271831
Elav-Gal4/+	24	0.735319049	0.144582684	0.144582684
CNMa-Gal4/UAS-Kir2.1	24	1	0.054577242	0.050314487
+/UAS-Kir2.1	24	0.416468213	0.110462499	0.100433134
CNMa-Gal4/+	24	1	0.076222246	0.076032166
CNMa-Gal4/UAS-AstC-IR1	24	1	0.063869939	0.059108427
+/UAS-AstC-IR1	24	0.050513268	0.120989153	0.110004029
CNMa-Gal4/+	24	0.999999999	0.129797767	0.129797767
$AstC^{01}/AstC^{01}$,*CNMa-Gal4/UAS-AstC*	24	0.00201599	0.327868612	0.199814842
$AstC^{01}/AstC^{01}$	24	0.203087958	0.225959468	0.213590708
$AstC^{01}/AstC^{01}$,*CNMa-Gal4/+*	24	1	0.034312483	0.030958631
dilp2-Gal4/UAS-AstC-R1-IR1	24	0.051882018	0.177480762	0.177480762
+/UAS-AstC-R1-IR1	24	0.17241216	0.224020162	0.178336026
dilp2-Gal4/UAS-AstC-R2-IR2	24	0.400527827	0.044579184	0.029692463
+/UAS-AstC-R2-IR2	24	0.00062636	0.264602416	0.219268049
dilp2-Gal4/+	24	0.019295392	0.4325243	0.331142239

* The normalized number of stage 8 follicles per female shown in Fig. S8 and Fig. 4 was subjected to the MetaCycle analysis

Table S2. Primers or oligonucleotides used in this study

Primer name	Sequence	Purpose
XhoI-pDONR221 forward	5′-gttctcgagatcgcggccagcttg	*CNMa-Gal4*
KpnI-pDONR221 reverse	5′-catggtaccggtccagcctgctttttgtac	*CNMa-Gal4*
KpnI-Gal4:VP16:Hsp70 forward	5′-gttggtaccaatcaaaatgaagctgctgagtagt	*CNMa-Gal4*
XhoI/XmaJI-LexA/Gal4-Hsp70 reverse	5′-cttctcgagcctaggctcgcgtatcggtgattcat	*CNMa-Gal4*
BglII-pDONR221 forward	5′-cgaagatcttggcgtaatcatggtcatagc	*CNMa-Gal4*
BglII-Kan/FRT reverse	5′-agaagatctccctagcgtaactctttccaga	*CNMa-Gal4*
KpnI-CNMaLA forward	5´-caaggtaccttcccaatcccactgatgac	*CNMa-Gal4*
KpnI-CNMaLA reverse	5´-actggtacctcaactgcggagaatca	*CNMa-Gal4*
BglII-CNMaRA forward	5´-tatagatctccgccctgtccgcg	*CNMa-Gal4*
BglII-CNMaRA reverse	5´-tccagatctgggatgtcctggcatcacct	*CNMa-Gal4*
CNMa LA forward	5´-ttcccaatcccactgatgacc	*CNMa-Gal4*
CNMa RA reverse	5´-gggatgtcctggcatcacct	*CNMa-Gal4*
AstC cDNA forward	5’-gcgcggccgcaaaatgatgaaattcgtgcag	*UAS-AstC*
AstC cDNA reverse	5’-gcgcggtaccgaacttacttcctaaagcaggag	*UAS-AstC*
AstC-1 sense	5′-cttcgcatatagacatggcccatcg	AstC mutant
AstC-1 antisense	5′-aaaccgatgggccatgtctatatgc	AstC mutant
AstC-2 sense	5′-cttcgggaacttacttcctaaagc	AstC mutant
AstC-2 antisense	5′-aaacgctttaggaagtaagttccc	AstC mutant
CNMa-1 sense	5´-cttcggtggcctgctcttaccaac	CNMa mutant
CNMa-1 antisense	5´-aaacgttggtaagagcaggccacc	CNMa mutant
CNMa-2 sense	5´-cttcggacgggccatggcgtctcc	CNMa mutant
CNMa-2 antisense	5´-aaacggagacgccatggcccgtcc	CNMa mutant
Rp49 forward	5’-gacgcttcaagggacagtatctg	RT-qPCR
Rp49 reverse	5’-aaacgcggttctgcatgag	RT-qPCR)
Krh1 forward	5’-gcccaaatatgaatccgctctacc	RT-qPCR
Krh1 reverse	5’-gtcgtcgcccttgttcatgta	RT-qPCR
AstC forward	5’-gaccgtgtttgccaggataat	PCR for AstC mutant confirmation
AstC reverse	5’-tgggttccggatattcttcc	PCR for AstC mutant confirmation
CNMa forward	5’-cggttcagagatcgaagtgg	PCR for CNMa mutant confirmation
CNMa reverse	5’-gctgggcatattggtcagtt	PCR for CNMa mutant confirmation
AstC in situ forward	5′-taccgacgccaatttcat,	AstC *in situ* probe
AstC in situ reverse	5′-tggtttgttgaaatgcttga.	AstC *in situ* probe

SI References

1. S. Kondo, *et al.*, Neurochemical organization of the Drosophila brain visualized by endogenously tagged neurotransmitter receptors. *Cell Rep.* **30**, 284-297.e5 (2020).
2. J. H. Park, A. J. Schroeder, C. Helfrich-Förster, F. R. Jackson, J. Ewer, Targeted ablation of CCAP neuropeptide-containing neurons of Drosophila causes specific defects in execution and circadian timing of ecdysis behavior. *Development* **130**, 2645–2656 (2003).
3. Y. J. Choi, G. Lee, J. H. Park, Programmed cell death mechanisms of identifiable peptidergic neurons in drosophila melanogaster. *Development* **133**, 2223–2232 (2006).
4. E. J. Rulifson, S. K. Kim, R. Nusse, Ablation of insulin-producing neurons in files: Growth and diabetic phenotypes. *Science* **296**, 1118–1120 (2002).
5. S. L. McNabb, *et al.*, Disruption of a behavioral sequence by targeted death of peptidergic neurons in Drosophila. *Neuron* **19**, 813–823 (1997).
6. C. Melcher, M. J. Pankratz, Candidate gustatory interneurons modulating feeding behavior in the Drosophila brain. *PLoS Biol.* **3**, 1618–1629 (2005).
7. T. Wen, C. A. Parrish, D. Xu, Q. Wu, P. Shen, Drosophila neuropeptide F and its receptor, NPFR1, define a signalling pathway that acutely modulates alcohol sensitivity. *Proc. Natl. Acad. Sci. U. S. A.* **102**, 2141–2146 (2005).
8. S. Renn, J. Park, M. Rosbash, J. Hall, P. Taghert, A pdf neuropeptide gene mutation and ablation of PDF neurons each cause severe abnormalities of behavioral circadian rhythms in Drosophila. *Cell* **99**, 791–802 (1999).
9. S. Terhzaz, P. Rosay, S. F. Goodwin, J. A. Veenstra, The neuropeptide SIFamide modulates sexual behavior in Drosophila. *Biochem. Biophys. Res. Commun.* **352**, 305–310 (2007).
10. D. H. Kim, *et al.*, Rescheduling behavioral subunits of a fixed action pattern by genetic manipulation of peptidergic signaling. *PLoS Genet.* **11**, 1–25 (2015).
11. K. Asahina, *et al.*, Tachykinin-expressing neurons control male-specific aggressive arousal in drosophila. *Cell* **156**, 221–235 (2014).
12. J. Y. Yu, M. I. Kanai, E. Demir, G. S. X. E. Jefferis, B. J. Dickson, Cellular organization of the neural circuit that drives Drosophila courtship behavior. *Curr. Biol.* **20**, 1602–1614 (2010).

13. A. C. von Philipsborn, *et al.*, Neuronal control of Drosophila courtship song. *Neuron* **69**, 509–522 (2011).
14. F. N. Hamada, *et al.*, An internal thermal sensor controlling temperature preference in Drosophila. *Nature* **454**, 217–220 (2008).
15. T. P. Wijesekera, S. Saurabh, B. Dauwalder, Juvenile hormone is required in adult males for Drosophila courtship. *PLoS One* **11**, 1–11 (2016).
16. S. Kondo, R. Ueda, Highly improved gene targeting by germline-specific Cas9 expression in Drosophila. *Genetics* **195**, 715–721 (2013).
17. K. J. T. Venken, *et al.*, Versatile P[acman] BAC libraries for transgenesis studies in Drosophila melanogaster. *Nat. Methods* **6**, 431–434 (2009).
18. A. C. Groth, M. Fish, R. Nusse, M. P. Calos, Construction of transgenic Drosophila by using the site-specific integrase from phage φC31. *Genetics* **166**, 1775–1782 (2004).
19. S. J. Gratz, *et al.*, Highly specific and efficient CRISPR/Cas9-catalyzed homology-directed repair in Drosophila. *Genetics* **196**, 961–971 (2014).
20. F. Heigwer, G. Kerr, M. Boutros, E-CRISP: Fast CRISPR target site identification. *Nat. Methods* **11**, 122–123 (2014).
21. N. Yapici, Y.-J. Kim, C. Ribeiro, B. J. Dickson, A receptor that mediates the post-mating switch in Drosophila reproductive behaviour. *Nature* **451**, 33–37 (2008).
22. R. Allemand, Les rythmes de vitellogenese et d'ovulation en photoperiode LD 12:12 de Drosophila melanogaster. *J. Insect Physiol.* **22**, 1031–1035 (1976).
23. D. Jia, Q. Xu, Q. Xie, W. Mio, W. M. Deng, Automatic stage identification of Drosophila egg chamber based on DAPI images. *Sci. Rep.* **6**, 1–12 (2016).
24. T. Flatt, T. J. Kawecki, Juvenile hormone as a regulator of the trade-off between reproduction and life span in Drosophila melanogaster. *Evolution* **61**, 1980–1991 (2007).
25. D. Žitňan, T. G. Kingan, S. J. Kramer, N. E. Beckage, Accumulation of neuropeptides in the cerebral neurosecretory system of Manduca sexta larvae parasitized by the braconid wasp Cotesia congregata. *J. Comp. Neurol.* **356**, 83–100 (1995).
26. E. Y. Kim, *et al.*, A role for O-GlcNAcylation in setting circadian clock speed. *Genes Dev.* **26**, 490–502 (2012).

27. S. J. Kwak, *et al.*, Drosophila adiponectin receptor in insulin producing cells regulates glucose and lipid metabolism by controlling insulin secretion. *PLoS One* **8**, 2–11 (2013).
28. C. A. Schneider, W. S. Rasband, K. W. Eliceiri, NIH Image to ImageJ: 25 years of image analysis. *Nat. Methods* **9**, 671–675 (2012).
29. P. Fichelson, A. Brigui, F. Pichaud, Orthodenticle and Kruppel homolog 1 regulate Drosophila photoreceptor maturation. *Proc. Natl. Acad. Sci. U. S. A.* **109**, 7893–7898 (2012).
30. N. A. Gidaszewski, M. Baylac, C. P. Klingenberg, Evolution of sexual dimorphism of wing shape in the Drosophila melanogaster subgroup. *BMC Evol. Biol.* 9 (2009)
31. G. Wu, R. C. Anafi, M. E. Hughes, K. Kornacker, J. B. Hogenesch, MetaCycle: An integrated R package to evaluate periodicity in large scale data. *Bioinformatics* 32, 3351–3353 (2016).